JOURNAL OF MECHANICAL ENGINEERING AND SCIENCES
ISSN: 2289-4659 e-ISSN: 2231-8380
VOLUME 18, ISSUE 3, 2024, 10161 - 10170
DOI: https://doi.org/10.15282/jmes.18.3.2024.5.0802

UNIVERSITI MALAYSIA PAHANG AL-SULTAN ABDULLAH

RESEARCH ARTICLE

Design and development of a high-power wideband multimode Tonpilz transducer for underwater applications

M. Hadeed[1,2], H. S. Bhatti[1,2*], M. S. Afzal[2], E. Vorathin[1], M. Abdullah[2], M. A. Asghar[2]

[1] Department of Mechanical Engineering, Universiti Teknologi PETRONAS, 32610 Seri Iskandar, Perak Darul Ridzuan, Malaysia
[2] Department of Mechanical Engineering, COMSATS University Islamabad, Wah Campus, 47010 Wah Cantt, Pakistan

ABSTRACT - A multimode transducer is preferred for its broader bandwidth compared to traditional single-mode transducers. However, developing a wideband multimode Tonpilz transducer that operates at lower frequencies poses significant challenges. This study aims to create a high-power multimode Tonpilz transducer operating at 12 kHz with enhanced wideband characteristics by optimising the head mass radius. The devised transducer structure effectively incorporates two vibration modes: longitudinal and flapping, with the most simplistic head mass structure to maximise the fractional bandwidth (FBW) significantly. Further optimisation ensures a maximum bandwidth without compromising the transmitting voltage response. The variation of head mass structure and its impact on the transducer's overall performance was investigated using finite element analysis and experimental analysis. The optimised head mass radius was determined to be 85 mm, resulting in a highest FBW of 91.6% and a TVR_{peak} of 146.96 dB re 1mPa/V. Furthermore, the fabricated model with a head mass radius of 85 mm also exhibited a resonance frequency of 12.6 kHz, demonstrating good agreement between the finite element simulation and the fabricated prototype. Thus, the experimental validation by developing a prototype transducer ensures the efficacy of proposed structural design improvements.

ARTICLE HISTORY
Received : 02nd May 2024
Revised : 23rd July 2024
Accepted : 31st July 2024
Published : 30th Sept. 2024

KEYWORDS
Tonpilz transducer
Finite element analysis
Underwater acoustics
Wide head mass

1. INTRODUCTION

A Tonpilz transducer is highly favoured in sonar applications due to its affordability, ease of use, and well-established efficiency [1]. It converts energy from one form to another, transmitting sound waves as a projector and receiving them as hydrophones. Its compact structure allows it to emit high-power acoustic waves [2]. However, a traditional Tonpilz transducer, usually narrowband, typically operates around its resonant frequency in the longitudinal mode [3]. This often fails to meet the requirements for a wide frequency bandwidth, as it relies solely on this resonance mode. To address this limitation, numerous research efforts have focused on enhancing the frequency range of transducers, including integrating the longitudinal mode with other vibrational modes to develop multimodal transducers [4]. Coates et al. [5] proposed integrating multiple excitation segments with varying resonant frequencies into a single Tonpilz transducer to combine two resonant modes. They also emphasised the challenges of designing acoustic transducers to attain high bandwidth. Butler et al. [6] implemented a system that employed several electrical signals on the Tonpilz transducer's drive section to broaden the frequency range, building upon the concept of multi-resonant transducers. Furthermore, Butler et al. [7] proposed a transducer design capable of processing complex broadband sonar signals in another study. This design employs aluminium or composite polymer material sandwiched between a radiating piston (head mass), central mass, and a piezoelectric stack, resulting in a double resonant, three-degree-of-freedom system. However, this design is based solely on the longitudinal mode. Kurt et al. [8] conducted a recent study exploring various design approaches for analysing the Tonpilz transducer but only examined the longitudinal mode. Moreover, Bai et al. [9] developed a longitudinal vibration transducer with a low resonant frequency by engraving helical slots on the surface of the front mass (hollow cylinder). The resonant frequency was calculated using the frequency equations derived from the transducer's circuit, but this work focused exclusively on the longitudinal mode, neglecting the effect of the flapping mode. Wei et al. [10] proposed a single-mode Terfenol-D Tonpilz transducer that utilises Terfenol-D as the driving material. The drive section of the transducer comprises four Terfenol-D rods, each wound with 1,300 turns of AC drive wire to excite the rods. The proposed transducer operates at a resonant frequency of 1 kHz. Similarly, Villalobos et al. [11] proposed a single-mode Tonpilz transducer for active SONAR transmission applications. The authors used the transducer as a projector and a calibrated hydrophone to detect the cavitation effect in the Tonpilz transducer. A switch-mode power amplifier was used to excite the transducer, which operates at 11.6 kHz.

Hu et al. [12] presented a low-frequency dual-mode flextensional transducer designed for broadband transmission signals. The broadband signals were obtained by coupling the radial vibration of Lead Zirconate Titanate (PZT), a commonly used piezoelectric ceramic material, with the flexural vibration of metal shells, resulting in an operational bandwidth of 1.5–4 kHz. Similarly, Zheng et al. [13] proposed a Class VII flextensional transducer using third-generation crystal as the driving material. Due to its outstanding electromechanical and piezoelectric properties, third-generation

***CORRESPONDING AUTHOR | H. S. Bhatti** | ✉ hamza_24001196@utp.edu.my

crystal (i.e., manganese) is preferred for its higher electro-acoustic conversion efficiency. From the results, the proposed transducer achieved a bandwidth of 2.3 kHz. Additionally, Liu et al. [14] proposed a superposition multimode transducer that combines a spring ring and a fluid cavity inside the transducer. The structure of the transducer was enhanced and developed based on simulation results, and its transmitting voltage response (TVR) and acoustic response were also investigated. However, the bandwidth of this transducer was limited to 2.75 kHz. On the contrary, the present study does not rely on any complex geometric changes, expensive material inclusions, or difficult-to-incorporate electrical signal manipulation, and it addresses the bandwidth limitation issue in a more simplistic manner. Developing a multimode Tonpilz transducer poses the primary challenge of creating simultaneous vibrations of the head mass in two distinct modes [15, 16]. Achieving optimal bandwidth in a transducer requires maintaining a significant frequency gap between its two vibration modes. However, this advantage can be offset by an unacceptable level of fluctuation within the TVR spectrum [17]. Modifying a particular drive phase's longitudinal mode resonant frequency is a significant task. In contrast, the frequency of the flapping mode is highly sensitive to the thickness of the head mass, considering adjustments towards or away from the frequency of the longitudinal mode [18]. Achieving a broader bandwidth necessitates a higher frequency flapping mode, frequently executed with an accelerated head mass thickness [19]. However, this can inadvertently improve the transducer's efficiency due to the proportional relationship between the quality factor and the burden of the top mass.

This study focuses on developing a multimode Tonpilz transducer to enhance wideband characteristics. The novelty of the proposed Tonpilz transducer lies in effectively incorporating two modes of vibration (longitudinal and flapping modes) by structural variations and optimising the side acoustic window length along with the head mass of the transducer. These structural enhancements aim to maximise the fractional bandwidth (FBW), ensuring superior performance. Additionally, the transducer is compact, making it suitable for integration into transducer arrays. The initial design of a prototype featuring a multimode transducer structure was finalised using finite element analysis (FEA). Various parameters were modified, including the thickness of the head and tail masses, their respective radii, the number of ceramic discs, and the thickness of the head mass cap. Subsequent optimisation efforts focused on maximising bandwidth while ensuring the desired level of TVR within a specific frequency range. Finally, a prototype of the refined model was constructed and examined to validate its overall performance.

2. MATERIALS AND METHODS

Employing the commercially available software package ANSYS 2021 R1, this section depicts a multimode transducer's initial 2-D finite element model, as shown in Figure 1(a). The initial transducer configuration comprises a head mass, drive section, decoupler, tail mass, and steel bolt utilised to assemble those components. The excitation of the transducer is achieved through a meticulously arranged stack of piezoceramic discs. These discs exhibit an antiparallel polarisation scheme, where the poling direction of each disc is purposefully oriented in opposition to its neighbouring element. The tail mass incorporates a partial cavity to achieve a more compact transducer design. This cavity strategically houses the pressure section in the tail mass, successfully reducing the general length of the transducer. The transducer is readily equipped with extra components, including an acoustic window (EPDM) and a decoupler meeting. The transducer functions as an EPDM at the frontal surface of the top mass, serving dual purposes: the surroundings of the water medium matched with the safety and impedance. In the housing, the tail mass prolonged collar strategically located a decoupler meeting to isolate the transducer. While the transducer is housed inside a casing for the packaging of the underwater array, it is excluded from the initial model of FEA for computational streamlining. This study employs a multimode transducer design comprising multiple components. Material properties specific to each component are detailed in Table 1 [20].

Table 1. Mechanical properties of multimode Tonpilz transducer components

Component	Material	Poisson's Ratio	Density (kg/m³)	Young's Modulus (GPa)
Head Mass	Aluminium	0.33	2,700	70
Tail Mass	Brass	0.34	8,520	115
Bolt	Alloy Steel	0.27	7,800	205
Decoupler	Stainless Steel	0.28	7,867	202
Acoustic Window	EPDM	0.35	1,360	0.740
Housing	Aluminium	0.32	2,700	73
Electrode	Copper Alloy	0.35	8,925	105
Bushing	Acetal	0.38	1,395	3.9
Drive Section	PZT4	-	7,800	-

An in-depth analysis was conducted using the FE method to explore how dimensional versions within the Tonpilz transducer influence its overall acoustic performance. In this evaluation, harmonic analyses were performed using the FE version to study the TVR of the transducer at the nodal role placed 295 mm from the emitting floor. The main design variables, including the head mass thickness, T_h and tail mass thickness, T_t, head mass radius, R_h and tail mass radius, R_t, head mass cap thickness, T_{hc}, and the outer, R_{co} and inner, R_{ci} radius of PZT, were studied. Figure 1(b) illustrates the 2-D axisymmetric model of the multimode Tonpilz transducer with the corresponding nomenclature for each design

variable. These variables are instrumental in determining the FBW. Previous research conducted by one of the authors has underscored the significant influence of these design variables on FBW [20].

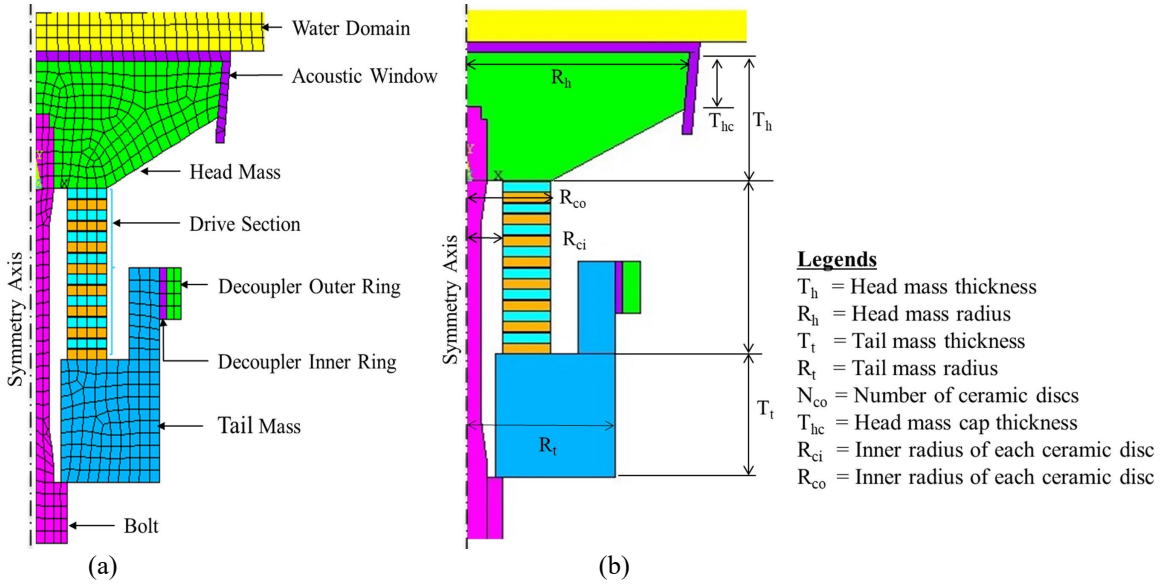

Figure 1. (a) A 2-D FE model of multimode Tonpilz transducer and (b) an axisymmetric model showing various design variables and their nomenclature

The parameters were kept constant after assessing their impact via FEA and considering realistic transducer fabrication and assembly constraints. The power segment consisted of PZT discs, each with a thickness, T_{pz} of 5 mm with an R_{ci} of 6 mm and R_{co} of 15 mm. The length, L_{tc} and, extended collar radius, W_{tc} of the tail mass are 21 mm and 5.5 mm, respectively. The radius of the inner, $W_{di,}$ and outer W_{do} decoupler is 3.25 mm and 1.5 mm, respectively, with lengths of 10 mm. The overall performance metrics under investigation included the peak frequency of TVR (f_{PTVR}), the height stage of TVR_{top}, and the bandwidth at -3 db. The frequency information was standardised for the initial model transducer resonant frequency.

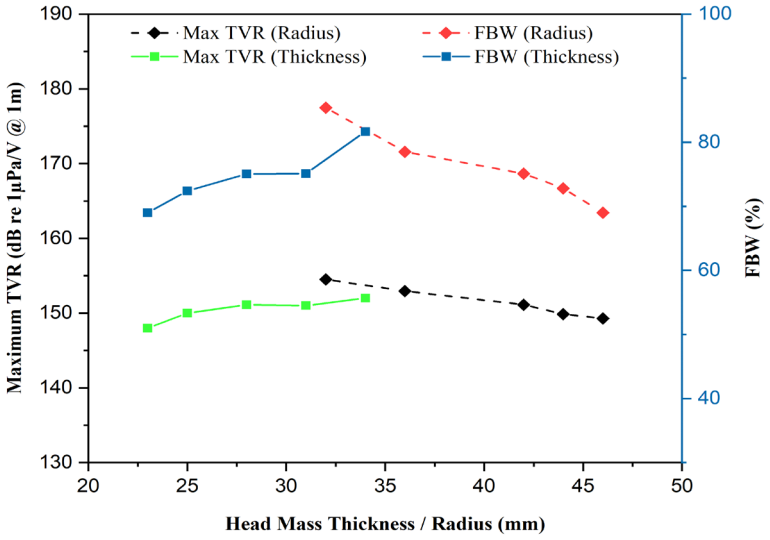

Figure 2. Variation of T_h and R_h on TVR_{peak} level and FBW

3. RESULTS AND DISCUSSION

3.1 Performance Characterization

The analysis discovered a decrease in the FBW and TVR_{peak} of the R_h. Conversely, there was an increase in the FBW and TVR_{peak} after examining the effect of these variations on the -3 dB FBW and peak TVR levels. Within the 22.5–35 mm thickness range, a steady increase in both FBW and TVR_{peak} could be observed, highlighting the interaction between these parameters. However, a sudden dip was observed in both vibration modes, and the -3 dB FBW was not analysed. Therefore, selecting this range ensures a comprehensive understanding of interaction points and avoids regions where response characteristics suddenly change. The peak FBW observed at approximately 85 mm R_h is likely attributed to the

significant interaction between flapping and longitudinal modes within the radius of the head mass, as shown in Figure 2. Next, another crucial design parameter, T_{hc} was examined. As the T_{hc} was varied, there was a corresponding increase in the TVR_{peak}, although not notably significant. However, an increase in T_{hc} caused a slow growth inside the transducer's FBW. The relationship between the TVR_{peak} and FBW in terms of the T_{hc} is provided in Figure 3. Then, the effects of T_t and R_t on the TVR_{peak} and FBW were examined (see Figure 4). Increasing T_t had a minimal impact on both TVR_{peak} and FBW. A higher T_t is likely to reduce f_{PTVR} due to increased transducer length. Similar to T_t, increasing R_t exhibited minimal influence on the TVR_{peak}. However, the FBW displayed a gradual increase with increasing R_t.

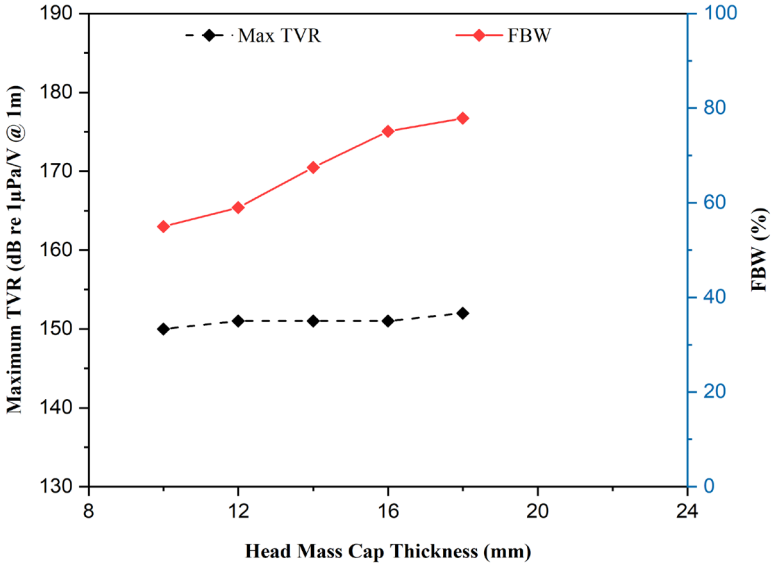

Figure 3. Variation of T_{hc} on TVR_{peak} level and FBW

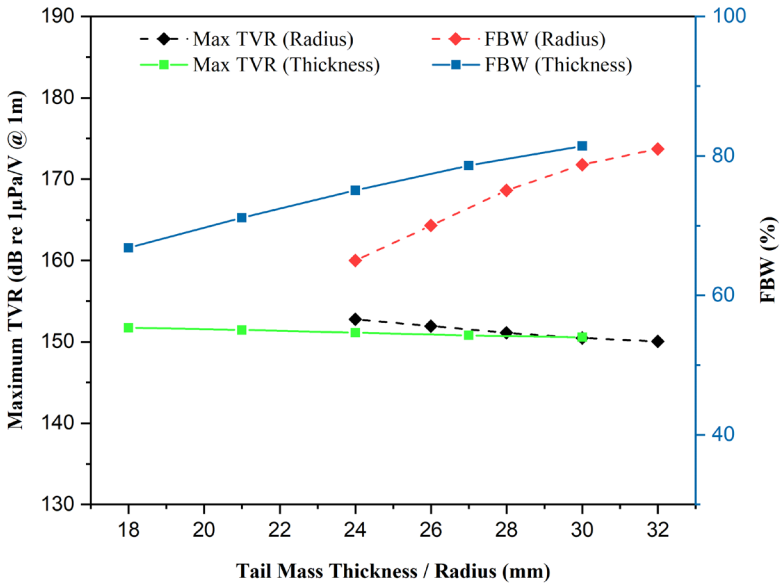

Figure 4. Variation of T_t and R_t on TVR_{peak} level and FBW

Lastly, the correlation between the inner, $R_{ci,}$ and outer, R_{co} radii of ceramic discs was examined (see Figure 5). The analysis revealed that as the outer radius increased, the TVR_{peak} gradually declined. Meanwhile, the FBW associated with the inner radius progressively increased with further increments in radius. Conversely, increasing the outer radius reduced the FBW and a slight uptick in the TVR_{peak}. A decrease in resonant frequency was observed when testing with lower ranges. When the radius was increased beyond this lower range, a decrease in the transducer's bandwidth was noted, indicating that the two modes were no longer combining.

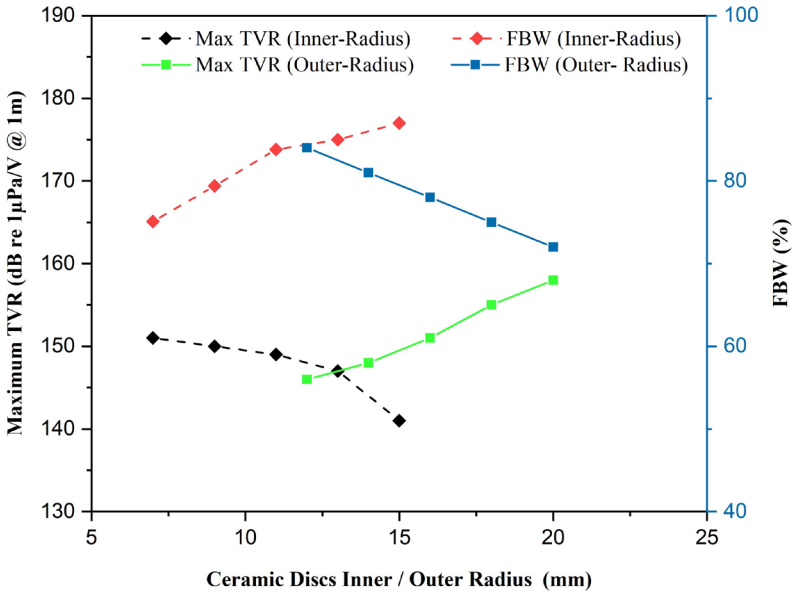

Figure 5. Variation of R_{ci} and R_{co} on TVR_{peak} level and FBW

3.2 Structural Optimization

For the optimisation of a Tonpilz transducer, the head mass radius plays an important role due to its wider thickness. Modifications to the transducer's shape were carried out using FEA to enhance the bandwidth of the structure, and the resulting impact on the overall structure was examined. Figure 6 illustrates a comparison between the initial model and the enhanced model, demonstrating an increase in the radius of both the head and tail mass. Initially, the T_t was 68 mm, and the T_h was 45 mm. Subsequently, adjustments were made, reducing the R_t to 45 mm and increasing the R_h to 65 mm.

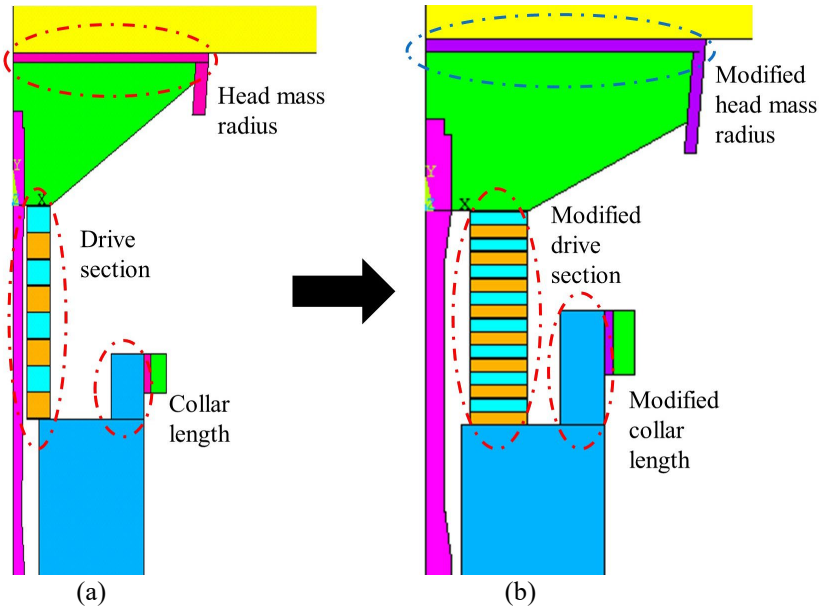

Figure 6. Comparison of (a) the initial model and (b) the enhanced model

Figure 7(a) illustrates the TVR spectrum of the initial model. At a frequency of 4.5 kHz, the peak represents the longitudinal mode of the transducer. Additionally, a peak at 13.5 kHz indicates the presence of the flapping mode. These peaks collectively define the operational bandwidth of the initial transducer model, with a TVR_{peak} of 144.2 dB re 1mPa/V. Figure 7(b) shows an impedance spectrum analysis that validates the 4.5 kHz frequency peak observed in the initial model. The FBW of the initial model was 57.6%.

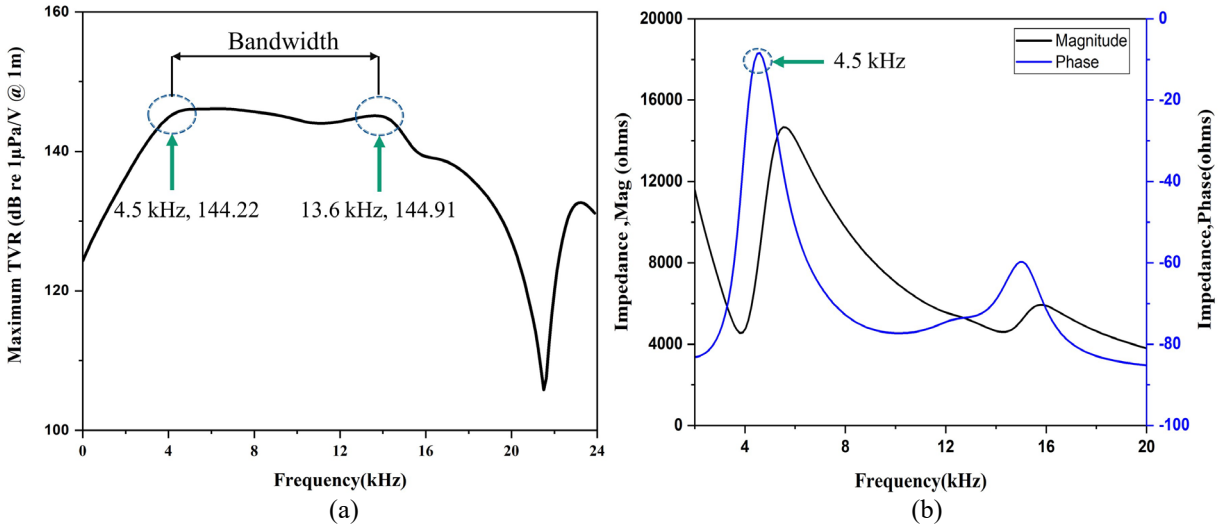

Figure 7. Initial model: (a) TVR spectrum and (b) impedance spectrum

To enhance the efficiency of the Tonpilz transducer, the entire model underwent optimisation by increasing the radius of the head mass. The initial step involved establishing the design variables' fundamental parameters and maintaining consistency with the initial model for simplicity. Analysing the head mass radius from 65 mm to 90 mm in 5 mm increments revealed crucial insights. Increasing the head mass radius from 65 mm to 70 mm did not achieve a -3 dB FBW due to misalignment between the two modes. The alignment of these modes is essential for achieving higher bandwidth. Similarly, increasing the head mass radius from 70 mm to 80 mm showed a similar trend. However, at 85 mm, a -3 dB FBW was successfully achieved, resulting in a bandwidth ranging from 12 kHz to 22.2 kHz. Further increasing the head mass radius to 90 mm again did not achieve a -3 dB FBW, indicating that the optimal bandwidth was achieved at a head mass radius of 85 mm. Figure 8 presents the TVR and spectrum of the enhanced and initial structures. The TVR is a pivotal parameter for assessing the correlation between the sound pressure and the voltage output produced by a transducer. In the context of concurrently evaluating longitudinal and flapping modes, the enhanced structure shows an increase in the peak TVR from the initial model's 144.2 dB re 1mPa/V to 146.96 dB re 1mPa/V, with the frequency range extending from 4.5 kHz to 12 kHz. Analysis of the TVR plot unveils resonance peaks occurring when the system's natural frequencies align with the applied frequencies, resulting in amplified vibration amplitudes. Additionally, the -3 dB FBW of the enhanced design indicates that the structural frequency has been enhanced to 12 kHz, marking a significant improvement of 4.5 kHz over the frequency of the initial model.

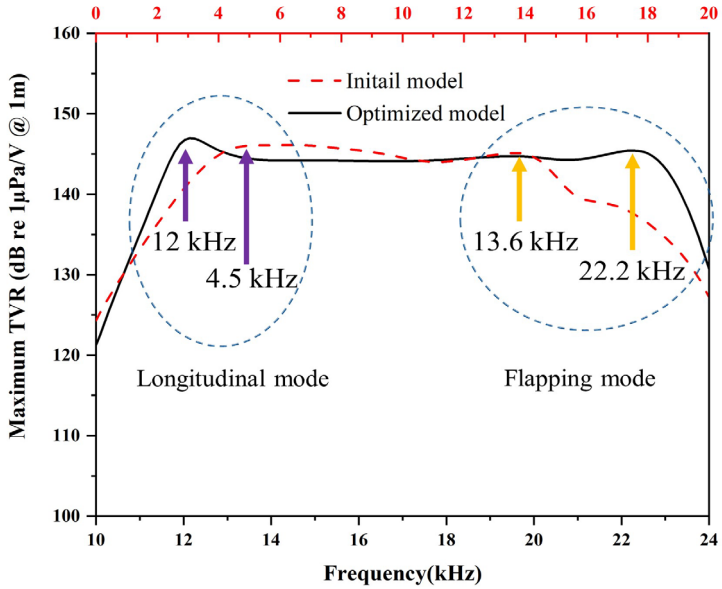

Figure 8. Comparison of the TVR spectrum between the initial and enhanced models

To validate the TVR response, Figure 9 presents a plot depicting impedance as a function of frequency. This plot illustrates both the magnitude and phase of the impedance spectrum. Specifically, the phase shows a resonant peak occurring at 12 kHz. Correspondingly, this peak in magnitude observed within the impedance spectrum aligns with a resonant frequency of 12 kHz. The Tonpilz transducer bandwidth significantly increased when comparing the finalised

and initial models. There is an approximate 34% increase in the FBW of the finalised structure, which is 91.6% when compared to the initial structure's 57.6%. The finalised model's actual bandwidth (f_2 - f_1) is 1.64f_o, representing a 105% increase above the basic model's bandwidth of 0.59f_o. Table 2 summarises a comparison of acoustic performance between the finalised and initial basic structures.

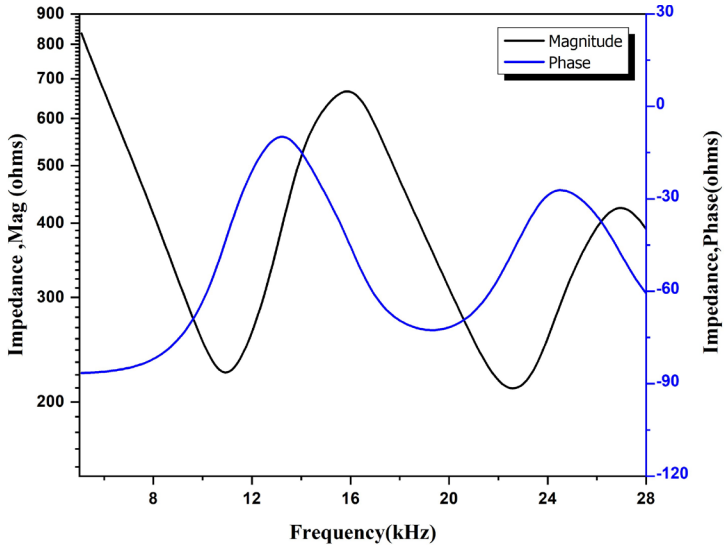

Figure 9. Improved model's impedance spectrum

Table 2. Comparison of acoustic performance between the finalised and initial models

Performance Factor	Finalised Configuration	Initial Configuration
TVR_{peak}	146.96	144.2
Lower bandwidth edge, f_1	0.97 f_o	0.73 f_o
Higher bandwidth edge, f_2	2.61 f_o	1.32 f_o
Bandwidth, (f_2 - f_1)	1.64 f_o	0.59 f_o
Efficiency of FBW (%)	91.6	57.6

3.3 Fabrication

To demonstrate the effectiveness of the design, an enhanced model of a multimode wideband transducer was manufactured. The Tonpilz transducer's construction involved using materials with specified properties outlined in Table 1. An illustration of the transducer's components in an exploded view is presented in Figure 10. At the top layer, the EPDM acoustic window with a thickness of 7 mm was modelled to create a surface that radiates in a circular shape. Even though the axisymmetric shape is intended for the head mass, both cases achieved identical acoustic traits due to the equal effective surface area as the EPDM.

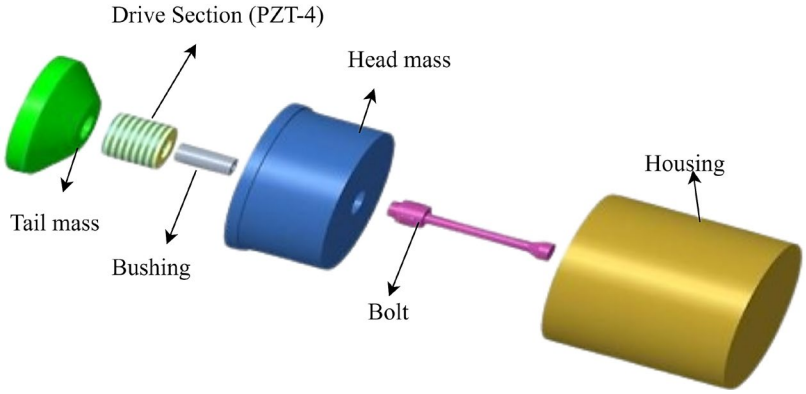

Figure 10. Exploded view of a multimode transducer

Firstly, a silicon rubber was applied to the side to create an acoustic separator, and the returned edges of the head mass were fabricated. A set of piezoceramic discs was stacked upon each other to form the pressure phase, and a copper electrode of 1 mm was placed between every two PZT during the assembly of the set. The organised bushings, inclusive of soft rubber and acetal, were then inserted inside the force section. Afterwards, the enhanced model of the tail mass was changed to a fabrication comprising a round hollow space. This alignment confirmed a reduction in the universal length

of the transducer in comparison to the traditional strong cylindrical shape, and a compact shape was also maintained. For the decoupler meeting, the inner ring of the EPDM was connected to the outer ring of the stainless steel. While driving the transducer, mechanical interference is prevented by the outer ring of the decoupler between it and the housing. After finalising the fabrication of the individual parts, the final model of the prototype transducer was changed to assembly. Firstly, the acoustic window was press-fitted on the pinnacle of the top mass. After the bolt was inserted during assembly, the PZT stack hooked up under the head mass with a bolt and its inner bushing. Figure 11 shows the finalised assembly without the housing. Fastening nuts were assembled with a bolt to complete the internal assembly. The electrical connections were made after the assembly was placed inside the housing.

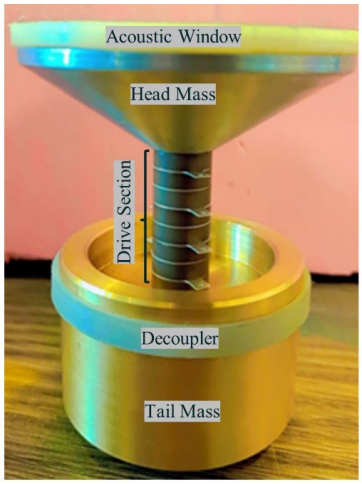

Figure 11. Assembled prototype of a multimode Tonpilz transducer

3.4 Experimentation of a Prototype Transducer Design

The fabricated prototype transducer's acoustic performance underwent an experimental evaluation to verify the design accuracy. This evaluation was then compared to the results predicted by the FEA simulation. The basic experimental setup involved using an impedance analyser with a fabricated Tonpilz transducer to obtain the output graph. The specific setup for this experiment is detailed in Figure 12.

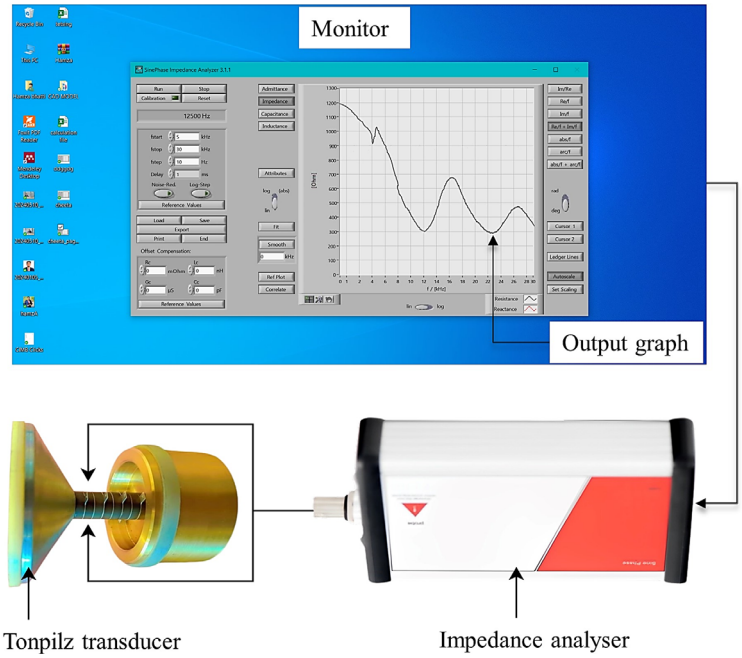

Figure 12. Schematics of the experimental measurement apparatus

The 262K sine phase impedance analyser model was used to measure the impedance spectrum of the Tonpilz transducer. The impedance spectrum reveals a resonant peak at 12.6 kHz. This peak in magnitude within the impedance spectrum corresponds to a resonant frequency of 12 kHz. The impedance spectrum of the multimode transducer at 12.6 kHz illustrates its relationship with varying frequencies, as Figure 13(b) illustrates. A frequency response comparison of a commercially available conventional transducer and the prototype transducer is shown in Figure 13. This comparison highlights the effectiveness of the multimode transducer over the conventional transducer structure of similar thickness

and frequency. The peak illustrated in Figure 9 and Figure 13(b) validates the correlation between the resonant frequency and the impedance spectrum in FEA and experimental analysis. This demonstrates a strong relationship between the two methodologies, thereby improving the overall bandwidth of the Tonpilz transducer.

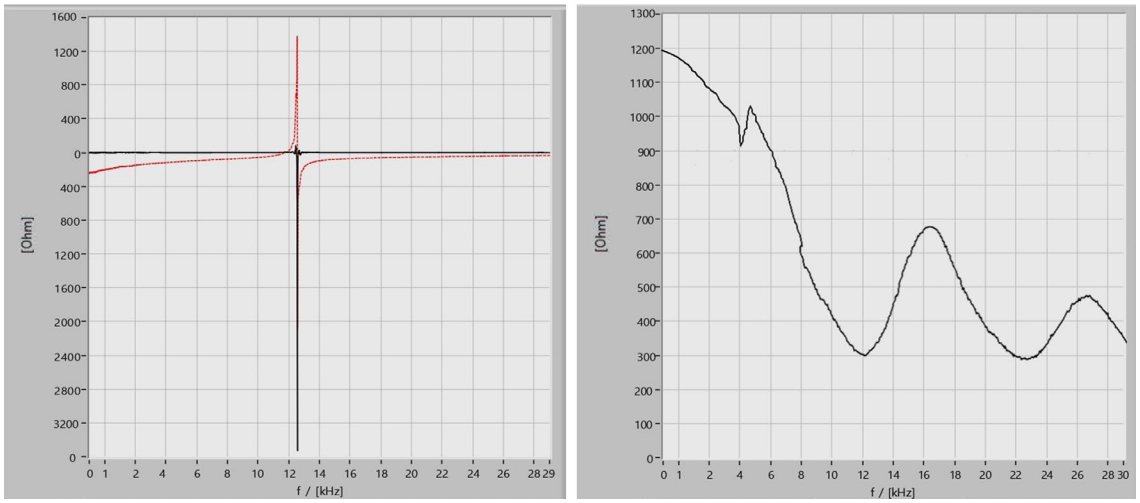

(a) (b)

Figure 13. Comparison of experimental results between (a) the conventional transducer structure and (b) the multimode prototype

4. CONCLUSIONS

This study successfully developed a high-power multimode (longitudinal and flapping) Tonpilz transducer operating at 12 kHz to achieve a high FBW. The primary conclusions of the present work are as follows:

i) An initial FBW of 57.6% was achieved with a TVRpeak of 144.2 dB re 1mPa/V at a head mass radius of 65 mm.

ii) Increasing the head mass radius from 70 mm to 80 mm did not result in a -3 dB FBW. This was due to the resonant frequencies of both the longitudinal and flapping modes not being optimally aligned. A similar trend was observed at a head mass radius of 90 mm, where the -3 dB FBW was not attained.

iii) The optimised head mass radius was determined to be 85 mm, resulting in the highest FBW of 91.6% and a TVRpeak of 146.96 dB re 1mPa/V.

iv) To validate the TVR response, the impedance spectrum as a function of frequency was considered, resulting in a peak resonant frequency of 12 kHz.

v) The fabricated model with a head mass radius of 85 mm exhibited an impedance frequency of 12.6 kHz, demonstrating good agreement between the FEA simulation and the fabricated model.

ACKNOWLEDGEMENTS

This work was supported by a research grant from TotalEnergies EP Malaysia allocated under the cost centre 015MD0-163. The authors would also like to thank Universiti Teknologi PETRONAS (UTP), Institute of Smart & Sustainable Living (ISSL), and Centre of Smart Infrastructure Modelling & Monitoring (SIMM) for their support in this research.

CONFLICT OF INTEREST

The authors declare no conflicts of interest.

AUTHORS CONTRIBUTION

H. S. Bhatti (Conceptualisation; Methodology; Data curation; Validation; Investigation; Formal analysis; Writing - original draft; Writing - review & editing)

M. Hadeed (Methodology; Data curation; Visualisation; Writing - original draft)

M. Abdullah (Methodology; Data curation; Visualisation; Software)

M. A. Asghar (Methodology; Data curation; Visualisation; Software)

M. S. Afzal (Conceptualisation; Methodology; Validation; Writing - review & editing; Supervision; Project administration; Resources)

E. Vorathin (Writing - review & editing; Visualisation; Funding acquisition; Supervision)

AVAILABILITY OF DATA AND MATERIALS

The data are available from the corresponding author upon reasonable request.

ETHICS STATEMENT

Not applicable.

REFERENCES

[1] E. Ringgaard, F. Levassort, K. Wang, J. Vaitekunas, H. Nagata, "Lead-free piezoelectric transducers," in *IEEE Transactions on Ultrasonics, Ferroelectrics, and Frequency Control,* vol. 71, no. 1, pp. 3-15, 2023.

[2] J. Y. Pyun, Y. H. Kim, K. K. Park, "Design of piezoelectric acoustic transducers for underwater applications," *Sensors*, vol. 23, no. 4, p. 1821, 2023.

[3] D. Stansfield, A. Elliott. Underwater Electroacoustic Transducers, 1st ed. California: Peninsula Publishing, 2017.

[4] K. Chen, T. Irie, T. Iijima, T. Morita, "Wideband multimode excitation by a double-parabolic-reflector ultrasonic transducer," *IEEE Transactions on Ultrasonics, Ferroelectrics, and Frequency Control*, vol. 67, no. 8, pp. 1620-1631, 2020.

[5] R. F. Coates, "The design of transducers and arrays for underwater data transmission," *IEEE Journal of Oceanic Engineering*, vol. 16, no. 1, pp. 123-135, 1991.

[6] J. L. Butler, A. L. Butler, "Stepped multiply resonant wideband transducer apparatus," Patent no. US 8,072843 B1, *United States Patent*, 2011.

[7] S. C. Butler, "Triply resonant broadband transducers," in *OCEANS'02 MTS/IEEE*, Biloxi, MI, USA, vol. 4, pp. 2334-2341, 2002.

[8] P. Kurt, M. Şansal, I. Tatar, C. Duran, S. Orhan, "Vibro-acoustic design, manufacturing, and characterization of a tonpilz-type transducer," *Applied Acoustics*, vol. 150, pp. 27-35, 2019.

[9] J. Bai, G. Zhang, X. Zhang, "A low-frequency longitudinal vibration transducer with a helical slot structure," *The Journal of the Acoustical Society of America*, vol. 145, no. 5, pp. 2948-2954, 2019.

[10] Y. Wei, X. Yang, Y. Chen, Z. Zhang, H. Zheng, "Modeling of high-power Tonpilz Terfenol-D transducer using complex material parameters," *Sensors*, vol. 22, no. 10, p. 3781, 2022.

[11] R. Villalobos, H. López, N. Vázquez, R. V. Carrillo-Serrano, A. Espinosa-Calderón, "Cavitation detection in a Tonpilz-type transducer for active SONAR transmission system," *Journal of Marine Science and Engineering,* vol. 11, no. 7, p. 1279, 2023.

[12] J. Hu, L. Hong, L. Yin, Y. Lan, H. Sun, R. Guo, "Research and fabrication of broadband ring flextensional underwater transducer," *Sensors*, vol. 21, no. 4, p. 1548, 2021.

[13] J. Zheng, S. Li, B. Wang, "Design and analysis of a broadband class VII flextensional transducer with the third-generation crystal, Mn: PIN-PMN-PT," *Sensors and Actuators A: Physical*, vol. 345, p. 113777, 2022.

[14] Q. Liu, J. Li, K. Yang, M.S. Wang, "Research on a multimode wideband Tonpilz transducer," in *16th Symposium on Piezoelectricity, Acoustic Waves, and Device Applications*, Nanjing, China, pp. 248-252, 2022.

[15] C. H. Sherman, J. L. Butler. Transducers and Arrays for Underwater Sound, 1st Ed. New York: Springer, 2007.

[16] B. Ji, Y. Lan, G. Qiao, M. Wang, "Bandwidth extension of the Tonpilz transducer using high-order longitudinal vibrations," *The Journal of the Acoustical Society of America*, vol. 154, no. 6, pp. 3709-3725, 2023.

[17] B.-C. Renner, J. Heitmann, F. Steinmetz, "AHOI: Inexpensive, low-power communication and localization for underwater sensor networks and μAUVs," *ACM Transactions on Sensor Networks (TOSN)*, vol. 16, no. 2, pp. 1-46, 2020.

[18] M. A. Jankauski, "Measuring the frequency response of the honeybee thorax," *Bioinspiration & Biomimetics*, vol. 15, no. 4, p. 046002, 2020.

[19] Z. Abdullah, S. Naz, M. A. Z. Raja, A. Zameer, "Design of wideband tonpilz transducers for underwater SONAR applications with finite element model," *Applied Acoustics*, vol. 183, p. 108293, 2021.

[20] M. S. Afzal, Y. Lim, S. Lee, H. Yoon, Y. Roh, "Optimization and characterization of a wideband multimode Tonpilz transducer for underwater acoustical arrays," *Sensors and Actuators A: Physical*, vol. 307, p. 112001, 2020.